Pergamon

Geochimica et Cosmochimica Acta, Vol. 68, No. 3, pp. 673–689, 2004

0016-7037/04 $30.00 + .00

doi:10.1016/S0016-7037(00)00452-6

Postshock annealing and postannealing shock in equilibrated ordinary chondrites: Implications for the thermal and shock histories of chondritic asteroids

ALAN E. RUBIN*

Institute of Geophysics and Planetary Physics, University of California, Los Angeles, CA 90095-1567, USA

(*Received February* 28, 2003; *accepted in revised form June* 24, 2003)

Abstract—In addition to shock effects in olivine, plagioclase, orthopyroxene and Ca-pyroxene, petrographic shock indicators in equilibrated ordinary chondrites (OC) include chromite veinlets, chromite-plagioclase assemblages, polycrystalline troilite, metallic Cu, irregularly shaped troilite grains within metallic Fe-Ni, rapidly solidified metal-sulfide intergrowths, martensite and various types of plessite, metal-sulfide veins, large metal and/or sulfide nodules, silicate melt veins, silicate darkening, low-Ca clinopyroxene, silicate melt pockets, and large regions of silicate melt. The presence of some of these indicators in every petrologic type-4 to -6 ordinary chondrite demonstrates that collisional events caused all equilibrated OC to reach shock stages S3–S6. Those type-4 to -6 OC that are classified as shock-stage S1 (on the basis of sharp optical extinction in olivine) underwent postshock annealing due to burial beneath materials heated by the impact event. Those type-4 to -6 OC that are classified S2 (on the basis of undulose extinction and lack of planar fractures in olivine) were shocked to stage S3–S6, annealed to stage S1 and then shocked again to stage S2. Some OC were probably shocked to stage ≥S3 after annealing. It seems likely that many OC experienced multiple episodes of shock and annealing.

Because ^{40}Ar-^{39}Ar chronological data indicate that MIL 99301 (LL6, S1) was annealed ~4.26 Ga ago, presumably as a consequence of a major impact, it seems reasonable to suggest that other equilibrated S1 and S2 OC (which contain relict shock features) were also annealed by impacts. Because some type-6 S1 OC (e.g., Guareña, Kernouvé, Portales Valley, all of which contain relict shock features) were annealed 4.44–4.45 Ga ago (during a period when impacts were prevalent and most OC were thermally metamorphosed), it follows that impact-induced annealing could have contributed significantly to OC thermal metamorphism.

1. INTRODUCTION

A common view of the thermal and shock histories of ordinary-chondrite (OC) parent bodies is that, for the most part, thermal metamorphism and shock metamorphism were distinguishable and successive events. For example, many workers (e.g., Bennett and McSween, 1996a; Keil, 2000) maintain that the decay of the short-lived radionuclide ^{26}Al heated chondritic planetesimals and that subsequent impacts (e.g., McSween, 1999) produced various shock effects in near-surface materials. It is widely recognized that impacts can produce significant localized heating (and even melting) of target rocks; this is true for asteroids (e.g., Fredriksson et al., 1963; Fodor and Keil, 1976; Wilkening, 1978; Taylor et al., 1979; Takeda et al., 1984; Bogard et al., 1995; Yamaguchi et al., 1998; Mittlefehldt and Lindstrom, 2001) and terrestrial impact craters (e.g., Floran et al., 1978; Grieve et al., 1980, 1987; Reimold et al., 1990; Schuraytz et al., 1994; Gibson and Reimold, 2003). Although thermal energy derived from nonadiabatic decay of the shock pressure generated by an impact can cause thermal metamorphism of rocks beneath the crater floor (Gibson, 2002), many workers believe that impacts on asteroids are incapable of causing thermal metamorphism of chondrites (e.g., Keil et al., 1997; McSween et al., 2002).

The primary method of discerning the degree of shock experienced by a chondrite is examination of its olivine grains (Stöffler et al., 1991). Olivine is readily affected by shock processes. It develops undulose extinction at shock pressures of <4–5 GPa (shock-stage S2), planar fractures at 5–10 GPa (stage S3), mosaicism at 10–15 GPa (stage S4), and planar deformation features at 25–30 GPa (stage S5) (Stöffler et al., 1991; Schmitt et al., 1994; Schmitt and Stöffler, 1995). At shock-stage S6 (45–60 GPa), olivine can undergo solid-state recrystallization, melting, or, under certain conditions, transformation into ringwoodite (a high-pressure phase with spinel structure). Some workers (e.g., Pellas and Storzer, 1981; Pellas and Fiéni, 1988; Pellas et al., 1990) have considered individual OC that possess olivine with sharp optical extinction to have never been significantly shocked.

However, shock-induced damage of the olivine crystal lattice can be repaired during annealing at subsolidus temperatures (Bauer, 1979; Ashworth and Mallinson, 1985). The possibility therefore exists that an OC could be shocked and annealed so that its olivine grains make the chondrite appear less shocked than it was at an earlier point in its history. If it was common on OC parent bodies for rocks to have been shocked and annealed, then some equilibrated OC (e.g., those of petrologic types 4 to 6) of low shock stage (S1 and S2) could contain evidence that these rocks once reached a higher shock stage than their olivine grains presently indicate. I call this hypothetical earlier shock stage the rock's maximum prior shock level.

2. ANALYTICAL PROCEDURES AND PETROGRAPHIC UNCERTAINTIES

I studied 210 petrologic-type-4 to -6 OC with published shock-stage values of S1 and S2. Thin sections of the chon-

* Author to whom correspondence should be addressed (aerubin@ucla.edu).

drites were examined microscopically in transmitted and reflected light; a search was made for petrographic shock indicators (see below). Grain sizes were measured microscopically using a calibrated reticle. The shock stage of each chondrite was checked against the published value; in each case, 10 or more olivine grains were examined. Seven meteorites (Acfer 010, Dar al Gani 283, FRO 90070, FRO 90108, FRO 90145, FRO 90160, FRO 95019) listed as stage S1 and two meteorites (FRO 90240 and FRO 95042) listed as stage S1–S2 in Grady (2000) were reclassified as S2. Hammadah al Hamra 044 and Dar al Gani 263 were classified as S2 in Grady (2000), but reclassified here as S1 on the basis of the sharp optical extinction in olivine. Jhung was classified as stage S3 in Bennett and McSween (1996b), but was reclassified here as S2 because of the paucity of planar fractures in olivine. Forrest 027, listed in Grady (2000) as L5/6, was reclassified as L6 because it contains some large (>50 μm) plagioclase grains. Hammadah al Hamra 027, classified as weathering stage W2 in Grady (2000), was reclassified here as W3 because of the extensive weathering of its metal grains.

There is no systematic bias in shock-stage classification between Stöffler et al. (1991) and me. Of the 21 OC whose shock-stage classification was determined both by Rubin (1994) and Stöffler et al. (1991), 19 are classified identically, one (Inman) was listed in Rubin (1994) as one shock stage lower and one (Elenovka) was listed as one shock stage higher than in Stöffler et al. (1991).

In the more weathered OC (W3-W6), numerous thin limonite weathering veins are present, making it difficult to identify chromite veinlets. In reflected light, many limonite veins appear almost identical in shade to chromite veinlets. Nevertheless, most chromite veinlets are composed of individual 0.5–5-μm-size blebs and/or ~0.5–1×5–10 μm-size needles, whereas the limonite veins tend to be continuous. Although for some weathered meteorites it is time-consuming to find unambiguous chromite veinlets, I identified such veinlets in every OC in this study.

In type-4 OC, chromite-plagioclase assemblages with low chromite/plagioclase modal abundance ratios are difficult to distinguish from patches of chromite-bearing mesostasis within porphyritic and barred chondrules. For the type-4 OC in this study, only those assemblages that occur within mafic silicate grains (rather than between them) or in the matrix were counted. Rapidly solidified metal-troilite blebs inside chondrules in type-4 OC were not considered to be shock products because they could have been produced by rapid cooling following chondrule formation.

Rapidly solidified metal-troilite intergrowths and metal±sulfide veins within 1 mm of the fusion crust were discounted as shock indicators because these features may have formed during atmospheric passage of the meteoroid host.

Zoneless plessite particles (Sears and Axon, 1975) were not considered shock indicators because they appear to have formed after peak OC metamorphic temperatures were reached by the supercooling of taenite grains below the taenite/taenite+kamacite solvus in the absence of heterogeneous kamacite nucleation sites (Reisener and Goldstein, 2003).

The high weathering stage of some of the rocks caused extensive to complete alteration of metallic Fe-Ni. This made it impossible to identify some potential shock indicators in these OC including silicate darkening, metal and troilite veins, rapidly solidified metal-troilite intergrowths, metal nodules, polycrystalline troilite, martensite, plessite, irregular grains of troilite within metallic Fe-Ni, and metallic Cu. Thus, the list of shock indicators in Tables 1 to 3 is a lower limit for the W3-W6 chondrites.

3. PETROGRAPHIC SHOCK INDICATORS

There are many petrographic shock indicators in equilibrated ordinary chondrites. With increasing degrees of shock, olivine develops undulose extinction, planar fractures, mosaicism and planar deformation features; low-Ca pyroxene develops undulose extinction, low-Ca clinopyroxene polysynthetic twin lamellae parallel to (100), mosaicism and planar deformation features; plagioclase develops undulose extinction, becomes partially isotropic, develops planar deformation features, and transforms into maskelynite (Stöffler et al., 1991). At high shock pressures, these silicate phases transform into high-pressure polymorphs (ringwoodite, majorite, and plagioclase with the hollandite structure, respectively) (Binns et al., 1969; Binns, 1970; Smith and Mason, 1970; Liu, 1978).

Additional shock effects in equilibrated OC include the development of mechanical twinning parallel to (001) and (100) in Ca-rich clinopyroxene (Ashworth, 1985), silicate darkening caused by the dispersion in silicate grains of curvilinear trails of small blebs of metallic Fe-Ni and troilite (Rubin, 1992; Leroux et al., 1996), chromite veinlets (Rubin, 1992), chromite-plagioclase assemblages (Rubin, 2003), metal and sulfide veins (e.g., Stöffler et al., 1991), narrow silicate melt veins (or glassy pseudotachylite-like veins) (Fredriksson et al., 1963), large metal and/or sulfide nodules (Widom et al., 1986; Rubin, 1995a, 1999), polycrystalline troilite (Bennett and McSween, 1996b), irregularly shaped troilite grains inside metallic Fe-Ni (Rubin, 1994), martensite and various types of plessite (e.g., Smith and Goldstein, 1977), rapidly solidified metal-sulfide intergrowths (Scott, 1982), metallic Cu grains (occurring mainly at metal-sulfide boundaries; Rubin, 1994), glassy melt pockets (Dodd and Jarosewich, 1979), and large regions of silicate melt (e.g., Bogard et al., 1995; Kring et al., 1996).

An important question to consider is whether all of these features necessarily indicate shock; it is conceivable that some features could have resulted from normal thermal metamorphism.

(1) McSween et al. (1978) heated samples of LL3.1 Krymka to 900°C–1000°C for 1 week and found that troilite had melted and penetrated fractures in the silicate grains. This demonstrates that high-temperature thermal metamorphism could potentially cause silicate darkening. However, as shown in Table 1, only 47% (16/34) of the shock-stage-S1, petrologic-type-6 OC exhibit silicate darkening. If this texture were a normal consequence of thermal metamorphism, it should occur in virtually all type-6 OC.

(2) It is possible that metal-sulfide veins could form in a thermally metamorphosed OC if the temperature exceeded that of the Fe-FeS eutectic (988°C); the engendered metal-sulfide melt could flow into fractures. However, such veins were found only in 26% (9/34) of the stage-S1, type-6 OC (Table 1). It is unlikely that these nine rocks were heated to higher-than-normal temperatures because they do not appear to be any more

Table 1. Petrographic shock indicators in shock-stage S1 type-5 and -6 ordinary chondrites.

Meteorite	Group/ type	Shock stage	Weath-ering stage	Chromite veinlets	cpa[a]	Metallic Cu	Irregular FeS in metal	Rapidly solidified metal-sulfide	Marten-site/ plessite	Polycryst-alline FeS	Metal-FeS veins	Silicate melt veins	Melt pockets	Silicate darkening	Low-Ca clino-pyroxene
Acfer 002	H5	S1	W3	+	+	+	+							+	
Acfer 046	H5	S1	W4	+	+									+	
Acfer 098	H5	S1	W3	+	+		+								
Acfer 100	H6	S1	W2	+	+		+							+	
Acfer 105	L6	S1	W2	+	+		+							+	
Acfer 118	L6	S1	W3	+	+		+								
Acfer 173	H6	S1	W0/1	+	+	+	+								
Acfer 196	H5	S1	W3	+	+	+	+								
Acfer 229	H5	S1	W4	+	+		+								
Acfer 258	H6	S1	W1	+	+		+								
Acfer 271	H6	S1	W1	+	+	+	+							+	
Acfer 314	H6	S1	W0/1	+	+	+	+								
Allegan	H5	S1	W0	+	+	+	+								
Bluewing 002	L5	S1	W4	+	+			+					+		
Bluewing 005	L5	S1	W2	+	+	+	+								
Dar al Gani 007	H6	S1	W0/1	+	+		+								
Dar al Gani 008	L6	S1	W3	+	+		+							+	
Dar al Gani 016	H5	S1	W4	+	+									+	
Dar al Gani 211	H6	S1	W2	+	+	+	+							+	
Dar al Gani 324	H6	S1	W1	+	+	+	+							+	
El Djouf 003	L6	S1	W4	+	+										
El Djouf 004	H6	S1	W0/1	+	+	+	+							+	
Estacado	H6	S1	W0	+	+				+						
Forrest 027	L6	S1	W4	+	+									+	
FRO 90001	H6	S1	W2	+	+			+			+			+	
FRO 90068	H6	S1	W3	+	+		+							+	
FRO 90075	H5	S1	W2	+	+			+						+	
FRO 90088	H6	S1	W2	+	+		+	+			+	+	+	+	
FRO 90136	H6	S1	W2	+	+		+	+			+				
FRO 90156	H6	S1	W1	+	+		+							+	
FRO 90172	L5	S1	W1	+	+		+			+					
FRO 90204	H6	S1	W2	+	+		+								
FRO 90221	H6	S1	W1	+	+		+	+			+				
FRO 90224	H6	S1	W3	+	+						+			+	
FRO 90236	H5	S1	W1	+	+		+								
FRO 90238	H5	S1	W2	+	+										
Guareña	H6	S1	W0	+	+	+	+			+					
Hughes 039	LL5	S1	W3	+	+		+								
Kernouvé	H6	S1	W0	+	+						+				
Lemmon[b]	H5	S1	W3	+	+		+								
MIL99301	LL6	S1	W1	+	+	+	+		+	+				+	+
Mundrabilla 013	H6	S1	W3	+	+									+	

(Continued)

recrystallized than other type-6 OC that lack metal-sulfide veins.

(3) It is also possible that silicate melt veins could form in an OC that was heated sufficiently to cause partial melting. However, only one of 34 stage-S1, type-6 OC (i.e., H6 FRO90088) contains such veins (Table 1). The fact that this chondrite contains numerous discernable chondrules away from the vein indicates that silicate melting was localized, consistent with an origin by shock. Furthermore, silicate melt veins were also identified in one stage-S1, type-5 OC (H5 Tanezrouft 001), inconsistent with the veins having formed by ultra-metamorphism.

(4) In principle, metallic Cu could form from melted metal-sulfide assemblages in OC that were heated above 988°C during thermal metamorphism. However, Rubin (1994) found that metallic Cu is no more abundant in type-6 OC than in type-4 OC, inconsistent with a high-temperature metamorphic origin. There is also a significant positive correlation in OC between shock stage and the number of occurrences of metallic Cu per mm^2 (Rubin, 1994).

Table 1. (Continued)

Meteorite	Group/ type	Shock stage	Weath- ering stage	Chromite veinlets	cpa[a]	Metallic Cu	Irregular FeS in metal	Rapidly solidified metal- sulfide	Marten- site/ plessite	Polycryst- alline FeS	Metal- FeS veins	Silicate melt veins	Melt pockets	Silicate darkening	Low-Ca clino- pyroxene
NWA 428[c]	L6	S1	W1	+	+	+	+			+	+				+
NWA 792	L5	S1	W1	+	+	+	+							+	
Oro Grande	H5	S1	W3	+	+								+		
Park[d]	L6	S1	W2	+	+										
Portales Valley	H6	S1	W0	+	+	+	+				+			+	
Red Dry Lake 002	H6	S1	W5	+	+										
Red Dry Lake 005	H6	S1	W6	+	+										
Sahara 97082	LL5	S1	W3–4	+	+										
Sahara 97097	LL6	S1	W3	+	+										
Superior Valley 005	H6	S1	W4	+	+										
Tanezrouft 001	H5	S1	W2	+	+		+				+	+	+		

[a] cpa = chromite-plagioclase assemblage.
[b] UCLA thin section 726 of Lemmon contains a 480-μm-diameter granular chromite-rich chondrule.
[c] NWA 428 also contains large (1-2-mm-size) troilite nodules.
[d] ASU thin section 1161B of Park contains a 400-μm-diameter barred chromite-rich chondrule and a 860-μm-diameter porphyritic chromite-rich chondrule.

(5) It is important to note that silicate darkening, metal-sulfide veins and silicate melt veins are much more abundant in highly shocked OC than in shock-stage S1 OC (Stöffler et al., 1991; Rubin, 1992). These arguments strongly suggest that these petrographic features are reliable shock indicators.

Approximate shock-stages can be assigned to each of these indicators. Mechanical twinning in Ca-rich clinopyroxene develops at shock-stage S4–S5 (Ashworth, 1985). Silicate darkening indicates S3–S6 (Rubin, 1992); chromite veinlets and chromite-plagioclase assemblages, S3–S6 (Rubin, 2003); metal and sulfide veins, S4–S6 (Stöffler et al., 1991); narrow silicate melt veins, S4–S6 (Stöffler et al., 1991); large metal and/or sulfide nodules, S4–S6 (Rubin, 1999); polycrystalline troilite, S4–S5 (Schmitt et al., 1993; Bennett and McSween, 1996b); irregularly shaped troilite grains inside metallic Fe-Ni, S3–S6 (Rubin, 1994); martensite, S4–S6 (e.g., Taylor and Heymann, 1970; Smith and Goldstein, 1977); rapidly solidified metal-sulfide intergrowths, S3–S6 (Scott, 1982); metallic Cu, S3–S6 (Rubin, 1994); and glassy melt pockets, S4–S6 (Dodd and Jarosewich, 1979; Stöffler et al., 1991). Impact-melt breccias (e.g., Cat Mountain, Chico, Rose City, Shaw, Smyer, Yanzhuang), which contain large regions of silicate melt, are considered to be shock-stage S6 (Stöffler et al., 1991). If several indicators are present in a rock, the shock stage can be assigned with increased precision. Although many shock indicators have a range of stage S3–S6, if the host rock is not an impact-melt breccia, the range of shock stages is S3 to S5.

Whereas annealing could potentially obliterate some shock effects (e.g., damaged olivine crystal lattices could be healed and fine-grained polycrystalline troilite could recrystallize), some shock indicators are very likely to survive moderate annealing. These include silicate darkening, chromite veinlets, chromite-plagioclase assemblages, metal and sulfide veins, large metal nodules, metallic Cu, and devitrified and recrystallized silicate melt veins (Rubin, 1992, 1994, 1999, 2002, 2003; Leroux et al., 1996). In addition, during annealing, martensite (an unstable body-centered-cubic phase) could unmix to form plessite.

4. RESULTS

4.1. Shock-Stage S1 Petrologic Type-5 to -6 Ordinary Chondrites

Grady (2000) listed the petrologic types and shock stages of 1432 highly metamorphosed (type-5 to -6) OC (including samples that are likely to be paired from meteorite-rich collecting areas, but excluding samples classified as type 7). In the combined set of type-5 to -6 OC, 7% are S1, 30% S2, 40% S3, 15% S4, 5% S5, and 3% S6.

I examined 53 type-5 and -6 OC (38 H, 11 L, 4 LL) of shock-stage S1 (Table 1). The low number of LL chondrites studied reflects the paucity of LL5-LL6 S1 chondrites; as of this writing, only seven are known.

On the bases of find location, chondrite group, petrologic type, texture and weathering stage (Wlotzka, 1993), it seems likely that some of these stones are paired. Possible pairings include the following: Acfer 002, 046, 196, 229 (H5, W3-W4); Acfer 173, 258, 271, 314 (H6, W0-W1); Acfer 105, 118 (L6, W2-W3); Dar al Gani 007, 324 (H6, W0-W1); FRO 90136, 90221 (H6, W1-W2); FRO 90156, 90204 (H6, W1-W2); and Red Dry Lake 002, 005 (H6, W5-W6). If all of these pairings are correct, then the number of type-5 and -6 S1 OC decreases to 28 H, 9 L and 4 LL.

All 53 stones contain ~0.05–1 vol% chromite-plagioclase assemblages (Table 1) varying in size from ~10–400 μm and consisting of 0.2–20-μm-size euhedral, subhedral, anhedral and rounded chromite grains surrounded by plagioclase or glass of plagioclase composition. Chromite veinlets also occur in each of the stones. The veinlets are typically 0.5–2 μm thick and 10–300 μm long.

Many of the less-weathered, shock-stage S1, petrologic

Table 2. Petrographic shock indicators in shock-stage S2 type-5 and -6 ordinary chondrites.

Meteorite	Group/ type	Shock stage	Weath-ering stage	Chromite veinlets	cpa[a]	Metallic Cu	Irregular FeS in metal	Rapidly solidified metal-sulfide	Marten-site/ plessite	Polycryst-alline FeS	Metal-FeS veins	Silicate melt veins	Melt pockets	Silicate darkening	Low-Ca clino-pyroxene
Acfer 010	L6	S2	W3	+	+					+				+	
Alkali	H6	S2	W2	+	+		+								
ALH88067	H6	S2	W1	+	+		+	+			+	+	+	+	
ALH88069	H5	S2	W1	+	+		+				+	+		+	
ALH88075	H6	S2	W1	+	+		+							+	
ALH88080	H5	S2	W1	+	+	+	+							+	
ALH88086	H5	S2	W1	+	+			+		+	+	+		+	
Alta'ameem	LL5	S2	W0	+	+	+	+	+							
Anlong	H5	S2	W0	+	+	+	+								
Boise City	L6	S2	W3	+	+										
Changde	H5	S2	W0	+	+	+	+								
Cuddeback Dry Lake 002	L6	S2	W4	+	+										
Cuddeback Dry Lake 004	H6	S2	W3	+	+		+								
Cuddeback Dry Lake 008	L6	S2	W3	+	+		+								
Cuddeback Dry Lake 010	L5	S2	W4	+	+										
Dar al Gani 283	L5	S2	W4	+	+									+	
Diamond Valley 001	H5	S2	W3	+	+										
Elbert	LL6	S2	W0	+	+						+	+		+	
Forest City	H5	S2	W0	+	+		+								
FRO 90108	H5	S2	W1	+	+		+								
FRO 90240	L6	S2	W2	+	+					+	+				
FRO 95019	H5	S2	W2	+	+			+							
FRO 95042	H5	S2	W1	+	+			+			+				
Glanerbrug[b]	L/LL5	S2	W0	+	+	+	+								
Harper Dry Lake 006	H6	S2	W5	+	+										
Harper Dry Lake 007	H5	S2	W4	+	+									+	
Innisfree	L5	S2	W0	+	+										
Jhung	L5	S2	W0	+	+		+		+					+	
Lucerne Valley 012	H6	S2	W3	+	+								+	+	
Lucerne Valley 013	L5	S2	W3	+	+									+	
Nazareth (e)	H6	S2	W3	+	+		+								
NWA 065	H5	S2	W4	+	+										
NWA 067	L6	S2	W5	+	+										
NWA 079	H5	S2	W2	+	+	+	+								
NWA 080	H5	S2	W5	+	+										
NWA 141	H5	S2	W1	+	+										
NWA 309	L5	S2	W3	+	+										
NWA 313	H5	S2	W3	+	+									+	
NWA 429	L6	S2	W3	+	+		+							+	
NWA 520	L5	S2	W3	+	+		+								
NWA 527	L5	S2	W1	+	+	+	+								

(Continued)

type-5 and -6 OC contain additional petrographic shock indicators (Table 1). These include silicate darkening, metallic Cu, irregular grains of troilite within metallic Fe-Ni (Fig. 1a), and rapidly solidified metal-troilite intergrowths (Figs. 1b,c), indicating that these rocks had maximum prior shock levels equivalent to stages S3–S6. Eleven of the S1 OC have metal-sulfide veins, three have polycrystalline troilite, and four have silicate-rich melt pockets, indicating maximum prior shock levels of S4–S5. Tanezrouft 001 (H5) contains chromite veinlets, chromite-plagioclase assemblages, irregularly shaped grains of troilite within metallic Fe-Ni, metal-sulfide veins, silicate melt veins, and silicate-rich melt pockets (Table 1). FRO 90088 (H6) contains a 200–350-μm-wide devitrified, mildly recrystallized silicate melt vein that extends across the entire 4-mm-wide thin section (Figs. 2a,b); a macroscopic dark shock vein (probably the same vein observed in thin section) is visible in

Table 2. (Continued)

Meteorite	Group/ type	Shock stage	Weath- ering stage	Chromite veinlets	cpa[a]	Metallic Cu	Irregular FeS in metal	Rapidly solidified metal- sulfide	Marten- site/ plessite	Polycryst- alline FeS	Metal- FeS veins	Silicate melt veins	Melt pockets	Silicate darkening	Low-Ca clino- pyroxene
NWA 660	H5	S2	W1	+	+	+	+								
NWA 669	L6	S2	W3	+	+										
NWA 674	L5	S2	W4	+	+										
NWA 712	L6	S2	W0	+	+		+								
NWA 720	LL6	S2	W2	+	+		+								
NWA 743[c]	L5	S2	W2	+	+	+	+						+		
NWA 780	LL6	S2	W0	+	+								+	+	
NWA 787	L6	S2	W1	+	+		+	+							
NWA 812	H5	S2	W5	+	+										
NWA 816	LL6	S2	W2	+	+	+	+								
NWA 822	H6	S2	W3	+	+		+			+					
NWA 916	L6	S2	W2	+	+		+								
NWA 924	H5	S2	W2	+	+	+	+								
NWA 985	H6	S2	W4	+	+										
NWA 1007	L6	S2	W1	+	+										
Ogi	H6	S2	W0	+	+	+	+								
Primm	H5	S2	W3	+	+										
QUE 97071	LL5	S2	W1	+	+										
Queen's Mercy	H6	S2	W0	+	+										
Rabbit Dry Lake	L6	S2	W5	+	+										
Red Dry Lake 003	H6	S2	W5	+	+		+							+	
Richardton	H5	S2	W0	+	+	+	+								
Ridgecrest	H5	S2	W2	+	+									+	
Roach	LL6	S2	W0	+	+										
Roundsprings	H5	S2	W5	+	+										
Saint-Séverin	LL6	S2	W0	+	+									+	
Silurian Dry Lake	LL6	S2	W3	+	+										
Silver Dry Lake 002	H6	S2	W4	+	+		+							+	
Songyyan	L6	S2	W1	+	+										
Spade[d]	H imb	S2	W1	+	+			+	+				+	+	
Superior Valley 006	H6	S2	W6	+	+									+	
Superstition Mountain	H5	S2	W4	+	+										
Tungsten Mountain 002	H6	S2	W5	+	+									+	
Tungsten Mountain 005	L6	S2	W3	+	+									+	
Tungsten Mountain 010	H5	S2	W3	+	+		+								
Tuxtuac	LL5	S2	W0	+	+										
Two Dot	H6	S2	W3	+	+		+								
Wagon Mound	L6	S2	W2	+	+		+						+		
Xingyang	H6	S2	W0	+	+										
Xi Ujimgin[1]	L/LL6	S2	W0	+	+										

[a] cpa = chromite-plagioclase assemblage.
[b] Classification change: In Grady (2000), Glanerbrug is classified as LL6 and Xi Ujimgin as L6.
[c] UCLA thin section 1056 of NWA 743 contains a 250×350 μm porphyritic chromite-rich chondrule.
[d] Spade is an H-chondrite impact-melt breccia.

the small (1.57-g) main mass of this rock (L. Folco, personal communication, 2003). This chondrite also exhibits silicate darkening and contains rapidly solidified metal-troilite intergrowths (Fig. 1b), metal-troilite veins, irregularly shaped grains of troilite within metal, chromite veinlets and chromite-plagioclase assemblages. Both Tanezrouft 001 and FRO 90088 experienced a maximum prior shock level equivalent to S4–S5.

Two shock-stage S1 equilibrated OC that have been studied in detail are Portales Valley (Kring et al., 1999; Rubin et al., 2001) and MIL 99301 (Rubin, 2002). Portales Valley (H6)

Table 3. Petrographic shock indicators in shock-stage S1 and S2 type -4 ordinary chondrites.

Meteorite	Group/ type	Shock stage	Weath- ering stage	Chromite veinlets	cpa	Metallic Cu	Irregular FeS in metal	Rapidly solidified metal- sulfide	Marten- site/ plessite	Polycryst- alline FeS	Metal- FeS veins	Silicate melt veins	Melt pockets	Silicate darkening	Low-Ca clino- pyroxene
Acfer 047	L4	S2	W2	+			+								
Acfer 199	L4	S2	W3	+			+	+							
Acfer 299	LL4	S2	W2	+			+								
Avanhandava	H4	S2	W0	+	+										
Bjurböle	L/LL4	S1	W0	+	+	+	+		+						
Dar al Gani 044	H4	S2	W2	+											
Dar al Gani 075	H4	S2	W4	+											
Dar al Gani 160	H4	S2	W4	+											
Dar al Gani 176	H4	S2	W4	+											
Dar al Gani 179	H4	S2	W4	+	+										
Dar al Gani 240	H4	S2	W4	+	+										
Dar al Gani 263	H4	S1	W4	+											
Dar al Gani 296	H4	S2	W4	+											
Forest Vale	H4	S2	W0	+	+	+	+								
FRO 90005	H4	S2	W1	+											
FRO 90018	H4	S2	W2	+											
FRO 90023	H4	S2	W2	+											
FRO 90031	H4	S2	W2	+	+										
FRO 90035	LL4	S2	W1	+				+							
FRO 90045	L4	S2	W1	+			+				+				
FRO 90047	L4	S2	W1	+											
FRO 90052	L4	S1	W1	+				+							
FRO 90070	L4	S2	W1	+				+							
FRO 90095	H4	S1	W3	+											
FRO 90098	H4	S2	W1	+	+										
FRO 90102	L4	S1	W1	+											
FRO 90135	LL4	S1	W1	+				+							
FRO 90145	LL4	S2	W1	+											
FRO 90159	H4	S1	W1	+											
FRO 90160	L4	S2	W1	+				+							
FRO 90164	L4	S1	W1	+											
FRO 90173	H4	S1	W2	+											
FRO 90177	H4	S2	W2	+											
FRO 90180	H4	S2	W1	+											
FRO 90183	H4	S2	W2	+											
FRO 93035	L4	S2	W1	+					+						
FRO 95017	H4	S1	W1	+	+										
FRO 97010	L4	S1	W1	+							+				
FRO 97023	H4	S1	W2	+	+		+								
FRO 97026	H4	S1	W2	+			+								
FRO 97048	H4	S1	W1	+	+		+								

(Continued)

exhibits silicate darkening and contains chromite-plagioclase assemblages, chromite veinlets, metallic Cu, irregular grains of troilite within metallic Fe-Ni, and thick metal veins with Widmanstätten patterns. The low modal abundances of chondrules and coarse mafic silicate grains in Portales Valley (e.g., 2.6 and 3.1 vol%, respectively, in one silicate clast) relative to normal H6 chondrites (11.4 and 9.8 vol%, respectively; table 2 of Rubin et al., 2001) imply that the meteorite was extensively melted. This is consistent with the apparent mafic-silicate overgrowths on relict chondrules. Rubin et al. (2001) interpreted Portales Valley as an impact-melt breccia (i.e., a rock that achieved a maximum prior shock level equivalent to stage S6) that experienced postshock annealing.

MIL 99301 (LL6) exhibits extensive silicate darkening and contains polycrystalline troilite, myrmekitic plessite, irregularly shaped grains of troilite within metallic Fe-Ni, relatively abundant metallic Cu, chromite veinlets and numerous chromite-plagioclase assemblages. There are also coarse grains of low-Ca clinopyroxene with polysynthetic twinning. Rubin (2002) concluded that MIL 99301 reached a

Table 3. (Continued)

Meteorite	Group/ type	Shock stage	Weath- ering stage	Chromite veinlets	cpa	Metallic Cu	Irregular FeS in metal	Rapidly solidified metal- sulfide	Marten- site/ plessite	Polycryst- alline FeS	Metal- FeS veins	Silicate melt veins	Melt pockets	Silicate darkening	Low-Ca clino- pyroxene
Hammadah al Hamra 021	H4	S2	W4	+			+								
Hammadah al Hamra 027	H4	S1	W3	+											
Hammadah al Hamra 044	H4	S1	W4	+	+										
Hammadah al Hamra 049	H4	S2	W3	+			+								
Hammadah al Hamra 086	H4	S2	W4	+											
Hammadah al Hamra 100	H4	S2	W3	+											
Hammadah al Hamra 118	H4	S2	W3	+		+	+								
Hammadah al Hamra 147	H4	S2	W2	+											
Hammadah al Hamra 184	H4	S2	W4	+											
Hammadah al Hamra 194	L4	S1	W0/1	+											
Hammadah al Hamra 195	L4	S1	W0/1	+		+	+								
Hammadah al Hamra 219	L4	S2	W3	+											
Imperial	H4	S2	W1	+	+										
Lucerne Valley 010	H4	S2	W3	+	+		+								
Menow	H4	S2	W0	+	+		+	+							
Nikolskoe	L4	S2	W0	+	+	+	+								
NWA 063	H4	S2	W3	+											
NWA 101	H4	S2	W1	+	+		+								
NWA 106	L4	S2	W3	+	+										
NWA 310	H4	S2	W5	+	+										
NWA 315	H4	S2	W1	+											
NWA 823	L4	S1	W2	+	+		+								
NWA 833	H4	S2	W3	+		+									
NWA 965	LL4	S2	W3	+				+	+						
NWA 991	LL4	S2	W3	+										+	
NWA 992	H4	S2	W1	+											
Red Dry Lake 006	H4	S2	W3	+	+			+							
Sahara 97138	LL4	S2	W3	+	+			+						+	
Ste. Marguerite	H4	S2	W0	+	+		+								
Saratov	L4	S2	W0	+		+	+								
Sheephole Valley	H4	S2	W2	+	+	+	+							+	
Superior Valley 010	L4	S2	W2	+											
Tungsten Mountain 003	H4	S2	W3	+	+		+								
UCLA 1436[a]	H4	S1	W4	+											

[a] Thin section number. A name for this stone has not yet been assigned by the Nomenclature Committee of the Meteoritical Society.

maximum prior shock level equivalent to shock-stage S4 before being annealed.

4.2. Shock-Stage S2 Petrologic Type-5 to -6 Ordinary Chondrites

I examined 81 type-5 and -6 OC (43 H, 26 L, 10 LL, 2L/LL) of shock-stage S2 (Table 2). The two chondrites designated L/LL (Glanerbrug and Xi Ujimgin) are intermediate in some of their properties between L and LL chondrites. The meteorites could be anomalous L chondrites, anomalous LL chondrites or members of a new OC group intermediate between L and LL (Kallemeyn et al., 1989; Rubin, 1990).

As in the S1 OC, similarities in find location, chondrite group, petrologic type, texture and weathering stage indicate

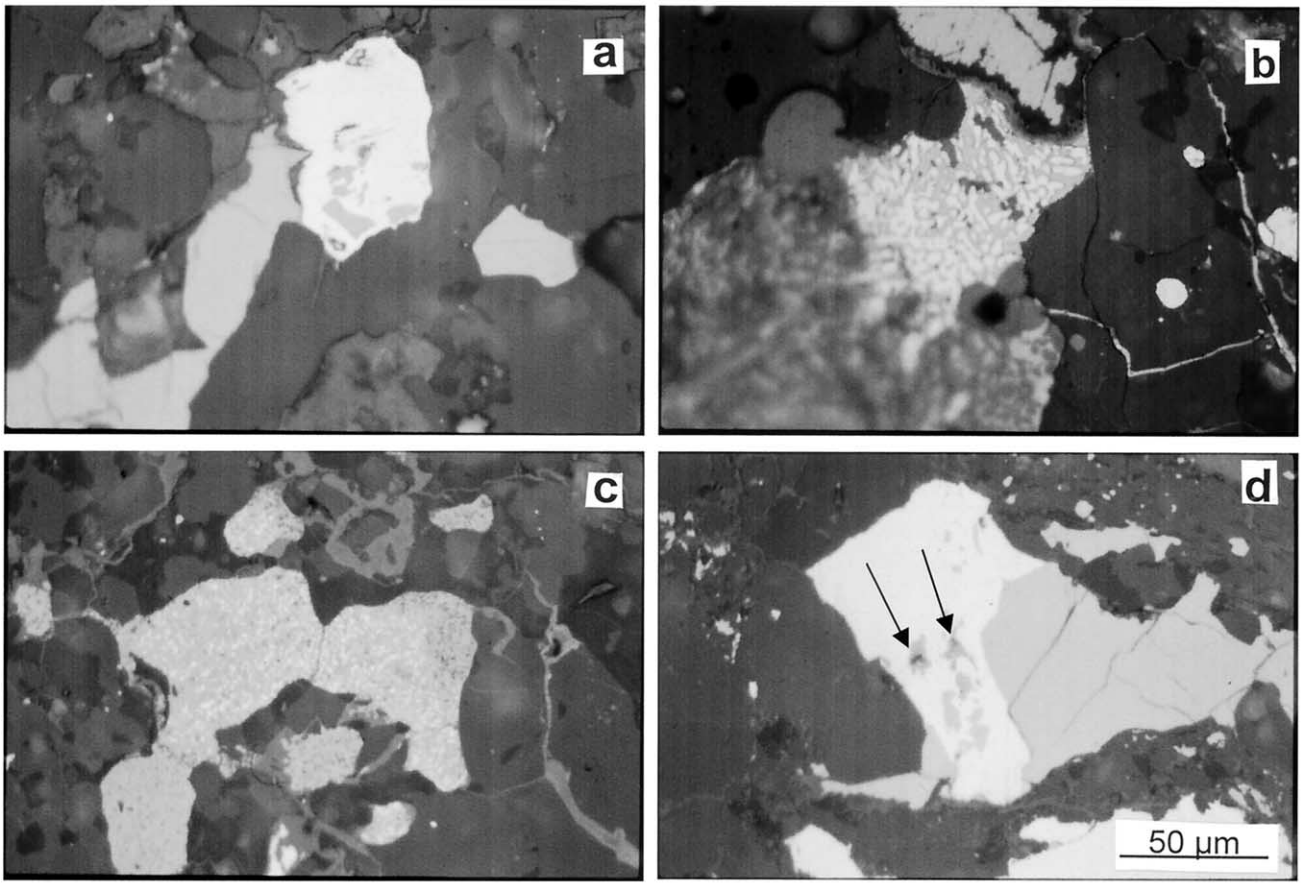

Fig. 1. Metallic Fe-Ni and troilite-bearing shock features. (a) Irregularly shaped grains of troilite (medium gray) inside metallic Fe-Ni (white) in FRO90156 (H6, S1). Large patch of troilite (medium gray) occurs at left. Field of view is 216 μm. (b) Rapidly solidified metal-troilite intergrowth in FRO90088 (H6, S1). Field of view is 216 μm. (c) Rapidly solidified metal-troilite intergrowth in FRO90001 (H6, S1). Field of view is 216 μm. (d) Metallic Cu grains (dark gray; arrows) adjacent to irregularly shaped troilite grains (medium gray) inside metallic Fe-Ni (white) in ALH88080 (H5, S2). Large patch of troilite (medium gray) occurs at right. Field of view is 216 μm. All images in reflected light.

that some of the S2 OC are likely to be paired. Possible pairings include the following: ALH88069, 88086 (H5, W1); Cuddeback Dry Lake 002, 008 (L6, W3-W4); NWA 065, 080 (H5, W4-W5); NWA 079, 141, 660, 924 (H5, W1-W2); NWA 822, 985 (H6, W3-W4); NWA 309, 520, 674 (L5, W3-W4); NWA 527, 743 (L5, W1-W2); NWA 712, 787, 1007 (L6, W0-W1); NWA 429, 669, 916 (L6, W2-W3); and NWA 720, 816 (LL6, W2). If these pairings are correct, then the number of type-5 and -6 S2 OC decreases to 37 H, 18 L, 9 LL and 2 L/LL.

All 81 stones contain chromite-plagioclase assemblages (Figs. 3a,b) and chromite veinlets (Fig. 3c). Thirty-five of the OC also contain irregularly shaped troilite grains within metallic Fe-Ni; 13 of these OC contain metallic Cu (Fig. 1d). These rocks reached maximum prior shock levels equivalent to stages S3–S6. Four stones (Acfer 010; ALH88086; FRO 90240; NWA 822) contain polycrystalline troilite, and six (ALH88067; Lucerne Valley 012; NWA 743, 780; Spade; Wagon Mound) contain silicate-rich melt pockets, indicative of maximum prior shock levels equivalent to stages S4–S6. Elbert (LL6) and ALH88067 (H6) exhibit silicate darkening and contain chromite veinlets, chromite-plagioclase assemblages, metal-sulfide veinlets and narrow silicate melt veins; ALH88067 also contains rapidly solidified metal-sulfide intergrowths and silicate-rich melt pockets (Table 2). These two stones experienced a maximum prior shock level equivalent to shock-stage S4 or S5.

Jhung exhibits silicate darkening and contains chromite veinlets, chromite-plagioclase assemblages and irregular grains of taenite in metallic Fe-Ni. Its maximum prior shock level was equivalent to stage S4–S5.

One shock-stage S2 OC that has been the subject of detailed study is Spade (Rubin and Jones, in press). Spade exhibits silicate darkening and contains chromite veinlets, chromite-plagioclase assemblages, abundant duplex plessite, rapidly solidified metal-troilite intergrowths, and silicate-rich melt pockets. The low modal abundances of relict chondrules (1.8 vol%) and coarse isolated mafic silicate grains (1.8 vol%) in Spade relative to normal H6 chondrites (11.4 and 9.8 vol%, respectively; Table 2 of Rubin et al., 2001) show Spade to be a rock that has been appreciably melted. Rubin and Jones (in press) concluded that Spade is an annealed impact-melt breccia that had reached a maximum prior shock level equivalent to shock-stage S6.

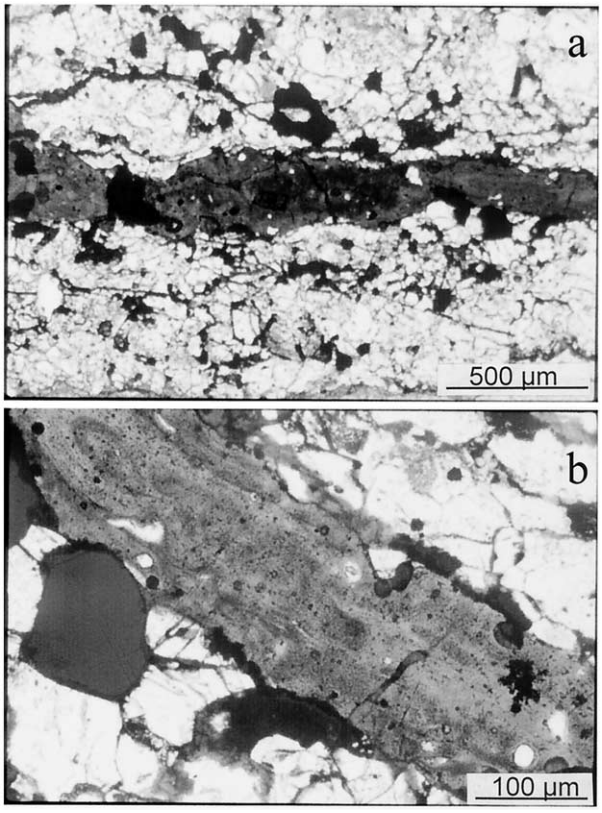

Fig. 2. Large, devitrified and mildly recrystallized silicate melt vein in FRO90088 (H6, S1). (a) Vein (dark gray) traversing silicate grains (light gray). The vein, which texturally resembles pseudotachylite veins, stretches across the entire thin section and must have originally been longer than 4 mm. Field of view is 2.16 mm. (b) Small portion of the vein. Field of view is 540 μm. Both images in transmitted light.

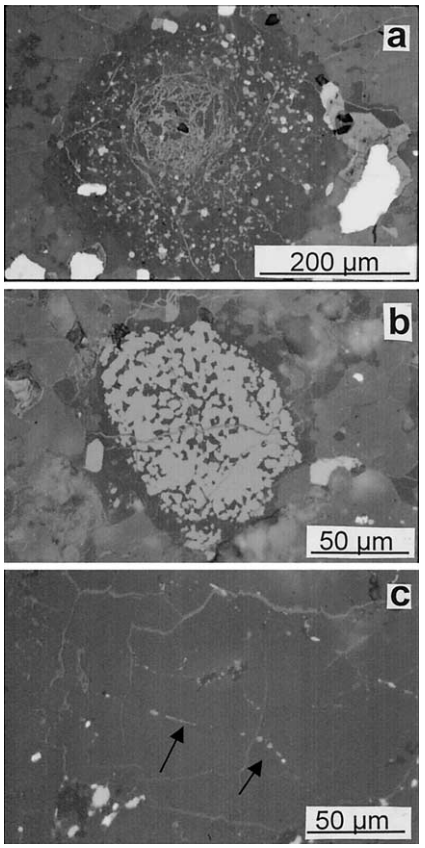

Fig. 3. Chromite-bearing shock features. (a) Large (400-μm-diameter) round chromite-plagioclase assemblages in ALH88075 (H6, S2). The main phases are chromite (light gray) and plagioclase (or glass of plagioclase composition) (dark gray). The light gray patch in the center of the assemblage is limonite formed by terrestrial weathering. Field of view is 540 μm. (b) Compact chromite-plagioclase assemblage in ALH88075 with a high chromite/plagioclase ratio. Field of view is 216 μm. (c) Chromite veinlets (light gray; arrows) traversing mafic silicate grains (medium gray) in ALH88080 (H5, S2). Field of view is 216 μm. All images in reflected light.

4.3. Petrologic Type-4 Ordinary Chondrites

I examined 76 type-4 OC (49 H, 19 L, 7 LL, 1 L/LL) of shock-stages S1 and S2 (Table 3). Possible pairings include Dar al Gani 160, 176, 179, 296 (H4, S2, W4); FRO 90005, 90098, 90180 (H4, S2, W1); FRO 90018, 90023, 90031, 90131, 90177, 90183 (H4, S2, W2); FRO 90045, 90070, 90160, 93035 (L4, S2, W1); FRO 97023, 97026 (H4, S1, W2); Hammadah al Hamra 021, 086, 184 (H4, S2, W4); Hammadah al Hamra 027, 044 (H4, S1, W3-W4); Hammadah al Hamra 049, 118 (H4, S2, W3); Hammadah al Hamra 194, 195 (L4, S1, W0/1); NWA 063, 833 (H4, S2, W3); NWA 101, 992 (H4, S2, W1); and NWA 965, 991 (LL4, S2, W3). If these pairings are correct, then the number of type-4 S1 and S2 OC decreases to 32 H, 15 L, 6 LL and 1 L/LL.

All of the stones contain chromite veinlets and 32% contain chromite-plagioclase assemblages, but the abundances of these objects in most type-4 OC are appreciably lower than in most type-5 and -6 OC (Table 4). Chromite veinlets are much more numerous and easier to identify than chromite-plagioclase assemblages. In many of the type-4 OC that contain chromite-plagioclase assemblages, the assemblages are rare and small.

Twenty-one of the type-4 OC contain irregularly shaped grains of troilite within metallic Fe-Ni, eight chondrites contain metallic Cu, and 12 contain rapidly solidified metal-sulfide assemblages.

Although the number of type-4 OC in this study is smaller than those of type-5 and -6 OC, there appears to be a dearth of type-4 chondrites that have high maximum prior shock levels. None of the type-4 OC listed in Table 3 has silicate melt veins, melt pockets, or polycrystalline troilite. I conclude that the type-4 OC studied here reached maximum prior shock levels equivalent to stages S3–S4.

5. DISCUSSION

5.1. Production of Petrographic Shock Indicators

To establish the case that equilibrated OC of shock-stage S1 have been shocked and annealed, it is necessary to demonstrate that the petrographic shock indicators in these rocks are reliable. It must be shown that the indicators could not occasionally form in unshocked rocks. There are two main arguments for the reliability of the shock indicators: (1) they occur most commonly in shocked OC, and (2) chromite veinlets and chro-

Table 4. Percentages of ordinary chondrites containing specific shock indicators.

Shock stage	S1	S2	S1 and S2
Petrologic type	5 and 6	5 and 6	4
Number of OC	53	81	76
Numbers in OC groups	38 H, 11 L,	43 H, 26 L,	49 H, 19 L,
(Possible pairings ignored)	4 LL	10 LL, 2 L/LL	7 LL, 1 L/LL
Chromite veinlets	100%	100%	100%
Chromite-plagioclase assemblages	100%	100%	32%
Metallic Cu	28%	16%	11%
Irregular troillite within metal	62%	43%	28%
Rapidly solidified metal-sulfide	13%	9%	16%
Martensite/plessite	2%	2%	3%
Polycrystalline troilite	6%	5%	0%
Metal-sulfide veins	21%	7%	3%
Silicate melt veins	4%	5%	0%
Melt pockets	8%	7%	0%
Silicate darkening	40%	28%	4%
low-Ca clinopyroxene	4%	0%	0%

mite-plagioclase assemblages (the two most common indicators) are associated in many shock-stage-S1 OC with other indicators that clearly require significant temperature excursions. These arguments are detailed below.

All of the shock indicators listed in Tables 1 to 3 occur most commonly in shock-stage S3–S6 chondrites. For example, chromite veinlets and chromite-plagioclase assemblages constitute ~3 vol% of Jartai (L6, S4) and ~1 vol% of Hualapai Wash (L6, S4). They are present in the shock-stage S6 impact-melt breccias Chico, Rose City, Smyer and Yanzhuang. In addition, Rubin (2003) reported them in several shock-stage S5 chondrites (L6 Alfianello, L6 Château-Renard, L5 Kingfisher, L6 Pinto Mountains, L6 Sixiangkou), many S4 OC (L4 Bald Mountain, H6 Charsonville, H5 Enshi, L5 Farmington, H4 Faucett, H5 Gilgoin, L4 Goodland, L3.7 Hedjaz, L6 Hualapai Wash, L6 Jartai, L6 La Criolla, H5 Lost City, L6 NWA 108, L6 Stratford, L6 Suizhou, H5 Zaoyang), and some S3 OC (L6 Barwell, H6 Butsura, LL6 Dhurmsala, H4 Farmville, H6 Lunan, H4 Mayfield, H5 Magombedze, H6 Mt. Browne, H6 Wuan, H6 Zhovtnevyi). The common occurrence of chromite veinlets and chromite-plagioclase assemblages in significantly shocked OC is consistent with their production during shock events.

Many petrographic shock indicators require melting. Melting of metal and troilite is necessary to produce metal-sulfide veins, rapidly solidified metal-troilite intergrowths and irregularly shaped troilite grains within metallic Fe-Ni. Temperatures must have reached or exceeded the Fe-FeS eutectic (988°C). Metallic Cu grains (e.g., Fig. 1d) form after localized shock-melting of metal-troilite assemblages at similar temperatures, crystallization of taenite, supersaturation of Cu in the residual sulfide-rich melt, and nucleation of small patches of metallic Cu at high-surface-energy sites (Rubin, 1994).

The rapidly solidified metal-troilite intergrowths in OC (Figs. 1b,c) require quenching following melting. These objects appear to have cooled at rates typically between 10^0 and 10^3 °C s^{-1} (Scott, 1982).

Silicate melting is required to form glassy melt pockets and melt veins (e.g., Fig. 2). Local temperatures in these rocks must have reached or exceeded the OC solidus temperature (~1100°C; Jurewicz et al., 1995). High temperatures must have been followed by rapid cooling to form the silicate glass. Although some glassy melt veins may have formed by localized frictional melting (e.g., Reimold and Colliston, 1994), such melting is a result of shock processes. The fact that some glassy melt veins in OC are associated with the high-pressure phases ringwoodite, majorite, $NaAlSi_3O_8$-hollandite, majorite-pyrope garnet and a high-pressure polymorph of merrillite (e.g., Binns et al., 1969; Binns, 1970; Coleman, 1977; Liu, 1978; Rubin and Read, 1984; Rubin, 1995; Xie et al., 2002) indicates that at least some cases of melt-vein formation are associated with high shock pressures.

Chromite-plagioclase assemblages (Figs. 3a,b) probably form by shock-melting of plagioclase (which has a low impedance to shock compression) followed by melting of adjacent chromite from heat from the plagioclase melt (Rubin, 2003). Temperatures probably reached ≥1100°C. Chromite grains completely surrounded by plagioclase within the assemblages tend to be richer in Al_2O_3 than unmelted chromite grains in the same chondrites. In shocked chondrites, most chromite grains not adjacent to plagioclase appear to be unmelted; this is in contrast to apparently melted chromite grains adjacent to plagioclase or within chromite-plagioclase assemblages.

Chromite veinlets (Fig. 3c) (which occur commonly in the vicinity of chromite-plagioclase assemblages) may form in a similar manner, i.e., by impact-melting of plagioclase, melting of chromite adjacent to the plagioclase melt, injection of a chromite-plagioclase melt into nearby fractures in mafic silicate grains, crystallization of chromite, and continued flow of the plagioclase melt until it encounters a void and pools to form a chromite-poor melt pocket.

The formation of these objects by localized heating and quenching are clearly attributable to shock processes. The shock indicators thus appear to be reliable.

5.2. Brecciation

Before the case can be established that equilibrated S1 OC were shocked and annealed, it is necessary to rule out brecciation as being responsible for juxtaposing shocked and un-

shocked material. Such juxtapositions can certainly occur: e.g., the Kendleton L-chondrite breccia contains L5 clasts of shock-stage ~S2 and silicate-darkened L4–5 clasts of shock-stage ~S4 (Ehlmann et al., 1988); the Zag H-chondrite regolith breccia contains H5 clasts of shock-stage S2 and H6 clasts of shock-stage S4 (Rubin et al., 2002). Furthermore, thin-section studies have shown that the majority of OC are fragmental breccias that contain some compositionally aberrant silicate and metallic Fe-Ni grains (Scott et al., 1985; Rubin, 1990). Some impact-melt-rock clasts and chromite-rich chondrules could also be incorporated into OC fragmental breccias as aberrant objects. Although these observations indicate that many OC are brecciated on subcentimeter scales, aberrant grains constitute <10 vol% of the OC whole rocks.

Brecciation cannot be responsible for shock-stage S1 OC exhibiting shock indicators common to rocks of higher shock stages because the olivine grains in the S1 OC that happen to be adjacent to shock indicators (e.g., chromite veinlets, chromite-plagioclase assemblages, polycrystalline troilite, martensite or plessite) exhibit the same optical properties (sharp optical extinction, no planar fractures, no planar deformation features) that are characteristic of unshocked material as do the other olivine grains in the same thin sections (Rubin, 2003).

5.3. Postshock Annealing

There are several rocks that clearly experienced extensive shock at earlier points in their history and that currently possess olivine grains with sharp optical extinction characteristic of shock-stage S1. These rocks include Portales Valley (interpreted as an impact-melt breccia that reached a maximum prior shock level equivalent to stage S6; Kring et al., 1999; Rubin et al., 2001) and MIL 99301 (an apparently unbrecciated rock that must have reached a maximum prior shock level equivalent to stage ~S4 on the bases of its metallic Cu, myrmekitic plessite, chromite veinlets, numerous chromite-plagioclase assemblages, and coarse grains of low-Ca clinopyroxene with polysynthetic twinning; Rubin, 2002). Silicate melt veins in FRO 90088 (H6) (Fig. 2) and Tanezrouft 01 (H5) and silicate-rich melt pockets in FRO 90088, Tanezrouft 001, Bluewing 002 (L5) and Oro Grande (H5) demonstrate that these rocks underwent localized silicate melting and quenching at an earlier point in their history. Oro Grande also contains a fine-grained impact-melt-rock clast that has the same mineral compositions as the H5 host (Fodor et al., 1972) and appears to have equilibrated with it. Saint-Séverin (LL6, S2) contains troilite melts that were injected into silicates by shock events and then annealed at high temperatures (Leroux et al., 1996).

The fact that these rocks now contain olivine with sharp optical extinction and no planar fractures implies that at some point after being extensively shocked, the rocks were annealed. Many coarse olivine grains in MIL 99301 exhibit extensive silicate darkening; they contain numerous intersecting curvilinear trails of tiny blebs of metallic Fe-Ni and sulfide situated along fractures in the olivine (e.g., figs. 4 and 7 of Rubin, 2002). Annealing healed the fractures in these olivine grains and sealed the trails of opaque blebs inside.

There is experimental evidence that olivine fractures can be annealed and that damage of the olivine crystal lattice can be healed at subsolidus temperatures. Elemental diffusion in olivine is relatively rapid (e.g., Buening and Buseck, 1973; Freer, 1981). Bauer (1979) showed that shock-induced olivine microfractures could be annealed in 20 min at 700–900°C. Ashworth and Mallinson (1985) annealed the shock-stage S5 Kyushu L6 chondrite for 90 h at 900°C and examined the olivine. They found that grain fractures had healed and that the preferred alignment of slip dislocations (common in unannealed specimens) had been lost due to slight changes in the orientation of the olivine crystal lattice. It seems plausible that lattice healing could also occur at lower temperatures over longer time periods.

Because every one of the shock-stage S1, petrologic type-4 to -6 OC in this study was shocked and annealed, generalizations are warranted. It appears that every equilibrated OC at one time or another was shocked to levels equivalent to stage S3 or above. Some of these rocks were annealed to stage S1; many were not appreciably annealed and retained their shocked characteristics. This same basic history transpired for all three OC groups.

The type-4 OC experienced a history similar to that of the type-5 and -6 OC except that the type-4 chondrites underwent (in many cases) less-intense shock and (in all cases) less-intense postshock annealing. Nevertheless, all of the S1 and S2 type-4 OC in this study appear to have reached maximum prior shock levels of at least S3, as have all of the S1 and S2 type-5 and -6 OC. There do not appear to be *any* unshocked equilibrated ordinary chondrites.

5.4. Postannealing Shock

There are several rocks that unambiguously experienced extensive shock at some point in their history but now possess olivine grains with undulose extinction and no planar fractures, characteristic of shock-stage S2. These include Spade, an impact-melt breccia that experienced appreciable melting and reached shock-stage S6, and Elbert (LL6), ALH88067 (H6) and ALH88069 (H5), chondrites with metal-sulfide veinlets and silicate melt veins that once reached shock-stage S4 or S5.

It seems unlikely that an OC shocked to stage S4–S6 could be annealed so precisely that its olivine would heal its planar fractures and planar deformation features, recrystallize and lose its mosaicism, but somehow retain undulose extinction (characteristic of stage S2). It is more probable that heating would be sufficient to reduce the strain of the olivine grains so that they would develop sharp optical extinction characteristic of shock stage S1. If this occurred, then Spade, Elbert, ALH88067, ALH88069 and the other type-4 to -6 S2 OC reached maximum prior shock levels equivalent to stages S3–S6, were subsequently annealed to stage S1, and then were (very weakly) shocked again to reach stage S2. The type-4 S2 OC were annealed sufficiently to heal the damaged olivine crystal lattices but insufficiently to cause large-scale recrystallization.

I conclude that all type-4 to -6 S2 OC experienced postshock annealing and postannealing shock.

Not all OC that underwent postannealing shock would be shocked to reach only stage S2. Some would experience more intense postannealing shock and reach stage S3 or higher. One such rock may be Appley Bridge (LL6, W0), listed as stage S2 in Grady (2000) but as S3 in Rubin (1994) because of the presence of planar fractures in olivine. Appley Bridge contains

chromite-plagioclase assemblages, chromite veinlets, metal veins, and devitrified silicate melt veins indicative of a maximum prior shock level equivalent to stage S4–S5.

Some OC could have undergone multiple episodes of shock and annealing. The petrologic types, volatile-element abundances and Ar release patterns of such rocks (e.g., Kunz et al., 1997) would reflect this complex thermal and shock history. These properties would not simply reflect an early epoch of thermal metamorphism as commonly assumed.

Ordinary chondrites that experienced multiple episodes of shock could potentially be identified by overlapping shock features. One such rock is Abernathy (L6, S4); this OC has a brecciated texture cross-cut by silicate melt veins (fig. 2a of Lambert et al., 1984).

5.5. Impact-Induced Annealing

Potential heat sources responsible for chondrite annealing include the decay of ^{26}Al (e.g., Reeves and Audouze, 1968; Grimm and McSween, 1993), the decay of ^{60}Fe (e.g., Shukolyukov and Lugmair, 1993; Mostefaoui et al., 2003), electromagnetic induction in the protosolar wind during an early T-Tauri phase (e.g., Sonett et al., 1970; Herbert and Sonett, 1979; Herbert, 1989; Herbert et al., 1991; Shimazu and Terasawa, 1995) and collisions, particularly those involving porous targets (e.g., Wasson et al., 1987; Cameron et al., 1990, 1991; Rubin, 1995b). Whereas all of these mechanisms could in principle have operated 4.5–4.6 Ga ago, only impacts could have caused heating significantly later. In the case of MIL 99301 (LL6, S1) (Rubin, 2002), postshock annealing occurred ~4.26 Ga ago (Dixon et al., 2003). At this late date, i.e., ~300 Ma after accretion, an impact event is the only plausible heat source; ^{26}Al would have long-since decayed away (more than 400 half-lives would have passed) and solar T-Tauri-type activity (postulated as a source of joule heating via electromagnetic induction) would have long-since ceased (Wood and Pellas, 1991).

In addition to MIL 99301, several LL chondrites have K-Ar or ^{40}Ar-^{39}Ar ages that cluster between 4.2 and 4.3 Ga: Alta'ameem (LL5, S2), 4.203 Ga; Tuxtuac (LL5, S2), 4.286 Ga; Uden (LL6, S2), 4.23 Ga; Trebbin (LL6 breccia, mainly S1), 4.20 Ga; a K-rich clast from Bhola (LL3–6 breccia, S2), 4.231 Ga; and, despite a complex age spectrum, Krähenberg (LL5, S2), ~4.2 Ga (Bernatowicz et al., 1988; Trieloff et al., 1989, 1994). These data suggest that there may have been a major impact event on the LL parent asteroid at that time that caused complete resetting of the K-Ar systematics (Trieloff et al., 1994). Uden (LL6) is a shocked and annealed, black OC (listed as LL7 in Grady, 2000) that has significant silicate darkening (Britt and Pieters, 1991), consistent with this collisional scenario. If the ages of these rocks reflect a major impact 4.2–4.3 Ga ago, then the model of Haack et al. (1996), that these rocks were all buried deeply within a very large asteroid that took 300 Ma to cool below the Ar closure temperature, is not applicable. The low shock stages (mainly S2) of these rocks indicate deep burial and concomitant annealing.

If impacts caused annealing in MIL 99301 and some of the other LL chondrites with similar K-Ar and ^{40}Ar-^{39}Ar ages, it is reasonable to suppose that impacts might be responsible for postshock annealing in additional shock-stage S1 and S2 petrologic type-4 to -6 OC.

If impacts are capable of causing postshock annealing at times significantly after accretion (as in MIL 99301, Alta'ameem and Tuxtuac), then it is plausible that impacts could also have caused annealing at earlier times when collisions were more prevalent, e.g., during the postaccretional period when most OC were thermally metamorphosed. This seems to have been the case for three S1 H6 chondrites: Guareña (which contains chromite veinlets, chromite-plagioclase assemblages, polycrystalline troilite and metallic Cu), Kernouvé (which contains chromite veinlets, chromite-plagioclase assemblages and metallic Fe-Ni veins), and Portales Valley (which contains chromite veinlets, chromite-plagioclase assemblages, metallic Cu and thick metallic Fe-Ni veins with Widmanstätten patterns); these rocks have maximum prior shock levels of S4–S5, S4–S5, and S6, respectively. The ^{40}Ar-^{39}Ar plateau ages of these OC are 4.44 ± 0.03, 4.45 ± 0.03 and 4.477 ± 0.016 Ga, respectively (Turner et al., 1978; Garrison and Bogard, 2001). If we make the alternative assumption that these rocks were heated by the decay of ^{26}Al, then their relict shock features remained unexplained.

Because these three OC were plausibly annealed by impacts during the general period of thermal metamorphism, it seems reasonable to conclude that impacts were a major mechanism of metamorphosing OC. This conclusion is consistent with other chondrite properties that point toward collisional heating:

(1) Annealed impact-melt-rock clasts occur in many OC fragmental breccias. This indicates that impact events occurred before or at the same time as thermal metamorphism and that the clasts were metamorphosed along with their hosts (Rubin et al., 1983).

(2) Unmelted chondritic clasts in OC impact-melt breccias are of high petrologic type (e.g., LL6 in Bison; L5 in Cat Mountain, L6 in Chico, H5 in Rose City, L6 in Shaw; H6 in Yanzhuang, LL6 in Y-790143; table 1 of Rubin, 1995b). This indicates that annealed chondritic material is physically associated with impact-melted material and may have been annealed by contact metamorphism.

(3) There is a positive correlation between petrologic type and shock stage among OC (Stöffler et al., 1991; Rubin, 1995b). Data from Grady (2000) on 1651 OC (which do not take possible pairings into account) show that the mean shock stage increases with petrologic type: type-3, S2.26 ($n=103$); type-4, S2.32 ($n = 240$); type-5, S2.64 ($n = 557$); type-6, S3.17 ($n = 751$). An illustration of these differences using the data in Grady (2000) is the comparison of the distribution of shock stages among type-3 OC (22.3% S1, 44.7% S2, 20.4% S3, 9.7% S4, 2.9% S5, 0% S6) and type-6 OC (6.8% S1, 18.8% S2, 42.3% S3, 19.3% S4, 8.0% S5, 4.8% S6).

Unequilibrated, type-3 chondrites tend to be richer in highly volatile species including rare gases, H_2O and In than more-metamorphosed chondrites (e.g., Zähringer, 1966; Marti, 1967; Heymann and Mazor, 1968; Tandon and Wasson, 1968). Stöffler et al. (1991) argued that the correlation between petrologic type and shock stage is due to the fact that porous, volatile-bearing type-3 OC would undergo whole-rock melting at appreciably lower shock pressures than OC of higher petrologic type. In other words, type-3 chondrites do not appear to be extensively shocked because any of these rocks that were

shocked would have been destroyed. However, some shocked type-3 chondrites do exist: Grady (2000) listed 10 type-3 OC of shock-stage S4 (Acfer 006, H3.7; FRO 90179, H3; Barratta, L3.8; Carraweena, L3.9; Felt (b), L3.5; FRO 90028, L < 3.4; Khohar, L3.6; Sahara 98323, L3.7; Tanezrouft 053, L3.8; Sahara 98175, LL3.5), one of stage S4–5 (Moorabie, L3.6) and three of stage S5 (FRO 90077, L3.8; FRO 90142, L3.8; Sahara 97193, L3.9).

Irrespective of the volatile contents of type-3 OC, there is little difference between the volatile contents of type-5 and -6 OC. Nevertheless, type-5 OC have a lower mean shock stage than type-6 OC indicating that the correlation between petrologic type and shock stage is valid.

(4) There is a significant correlation ($r = 0.96$; $n = 3$) between the proportion of highly metamorphosed members among the three OC groups and the degree of shock among members of these groups. The data of Grady (2000) show that 26% (1789/6880) of H chondrites, 67% (4075/6116) of L chondrites, and 41% (415/1022) of LL chondrites are petrologic type 6 or 7. Among those OC in Grady (2000) with published shock stage values, 7% (75/1046) of H chondrites, 42% (298/718) of L chondrites, and 10% (15/151) of LL chondrites are of shock-stage S4–S6. The L-chondrite group, which has the highest proportion of highly annealed members, also has the highest proportion of highly shocked members. H chondrites have the lowest proportion of highly annealed members and the lowest proportion of highly shocked members. (The more extensive shock in L chondrites is reflected in the exclusive or near-exclusive occurrence of the high-pressure phases ringwoodite and majorite within and adjacent to silicate melt veins in L6 chondrites; Rubin, 1985.)

(5) Those chondrite groups with many highly metamorphosed members (H, L, LL, EH, EL, CK) also have shocked members of stage ≥S4, whereas chondrite groups with no highly metamorphosed members (CI, CM, CO, CR) have no shocked members of stage ≥S4 (Rubin, 2002). CV chondrites follow the trend with a single exception: there are no highly metamorphosed members, but there is one CV chondrite (Efremovka) of shock-stage S4 (Scott et al., 1992). R chondrites also follow this trend; there are few metamorphosed members and few members of shock-stage ≥S4 (Grady, 2000). Nevertheless, some R chondrite breccias contain highly metamorphosed R5-R6 clasts and significantly shocked R-chondrite clasts (Kallemeyn et al., 1996).

Although it could be argued that the high bulk water contents of CI, CM and CR chondrites (16.9, 10.4, and 5.7 wt% H_2O, respectively; Mason and Wiik, 1962; Jarosewich, 1990) would cause shocked members of these groups to be destroyed via explosive volatile expansion, this argument cannot be applied to CO and CV chondrites, which have relatively low water contents (0.22 wt% in Kainsaz and 0.25 wt% in mean CV falls; McSween, 1977; Jarosewich, 1990). CO and CV chondrites should thus survive shock metamorphism, but, except for S4 Efremovka, there are no known highly shocked members of these groups.

These five arguments support an association between thermal metamorphism and shock metamorphism.

Impact heating cannot be a global process (Keil et al., 1997; McSween et al., 2002). It seems plausible, however, that annealing could occur in rocks buried beneath the floor or lining the walls of an impact crater or deposited in a hot, thick ejecta blanket. In low-density, high-porosity targets, most impacted material is driven into the crater floor and walls; relatively little is ejected (e.g., Housen, 2003; Housen and Holsapple, 2003). In porous asteroids, collisional kinetic energy is distributed through relatively small volumes of material (Stewart and Ahrens, 1999) and efficiently converted into heat in the crater vicinity (Melosh, 1989; Housen and Holsapple, 1999). Because burial at a moderate depth was necessary to cause annealing, at least one additional impact event was required to excavate the annealed OC and launch them from their parent body. Repeated impacts could cause individual batches of OC material to experience multiple episodes of shock and annealing. This scenario is consistent with the occurrence of type-4 to -6 OC of shock-stage S2; these rocks appear to have been shocked, annealed and shocked again.

Approximately 97% of OC falls are petrologic type 4 to 6 (Grady, 2000). In order for these rocks to have been thermally metamorphosed by impacts early in solar-system history, their parent asteroids must have been intensely battered. Alternatively, the type-4 to -6 OC that fall as meteorites are impact products that may have been rendered denser and tougher (i.e., more likely to survive space erosion and atmospheric passage) than less-battered material. Collisions could have made initially porous rocks denser by collapsing pores (Housen and Holsapple, 2003) and tougher by causing minor melting along grain boundaries (Bischoff et al., 1983).

5.6. Petrographic Constraints on Heating Timescales

Thermal models of OC asteroids heated by the decay of ^{26}Al (e.g., Bennett and McSween, 1996a; Ghosh and McSween, 2000; McSween et al., 2002) show elevated temperatures in type-4, type-5, and, particularly, type-6 materials for millions of years. In contrast, annealing times for rocks buried beneath the floors of impact craters or deposited in hot, thick ejecta blankets can be far shorter.

The shock-stage S1 chondrites FRO 90001 (H6), 90075 (H5) and 90088 (H6) contain olivine grains with sharp optical extinction that exhibit darkening due to the inclusion of curvilinear trails of metal and sulfide blebs. The Mg and Fe cations in the olivine grains need to diffuse only short distances to heal the damaged crystal lattice. In contrast, obliteration of the rapidly solidified metal-sulfide intergrowths in these chondrites (Table 1) would require much more extensive diffusion and metal-sulfide recrystallization. The occurrence of olivine grains with sharp optical extinction in the vicinity of rapidly solidified metal-sulfide intergrowths is consistent with short annealing times. The decay of ^{26}Al would cause such prolonged heating in the H-chondrite asteroid that the rapidly solidified metal-sulfide intergrowths in these chondrites would not have survived.

5.7. Evaluation of Thermochronologic Data Supporting ^{26}Al Heating

Recent thermochronological data on low-shock-stage H4–6 chondrites show that H6 chondrites have younger ^{40}Ar-^{39}Ar ages and slower ^{244}Pu fission-track cooling rates than H4 and H5 chondrites (Trieloff et al., 2003). These data were inter-

preted to indicate that H6 chondrites were buried more deeply than H4–5 chondrites in an "onion-shell" parent asteroid and that ^{26}Al was the most probable heat source. However, whereas Trieloff et al. plotted seven H chondrites in their inverse correlation of petrologic type and ^{244}Pu fission-track cooling rate, Taylor et al. (1987) determined metallographic cooling rates of 20 H chondrites and found no significant correlation with petrologic type (the correlation coefficient r = -0.13). Because metallographic and fission-track cooling rate studies of the same meteorites yield consistent results (fig. 4 of Taylor et al., 1987), it seems prudent to accept the larger data set of Taylor et al. and conclude that there is no correlation between petrologic type and cooling rate.

The inverse correlation of ^{40}Ar-^{39}Ar age and petrologic type found by Trieloff et al. (2003) for eight H chondrites indicates that the more-metamorphosed chondrites were more deeply buried and took longer to reach Ar closure temperatures. This correlation does not mandate a specific heat source. Although Trieloff et al. (2003) advocated the decay of ^{26}Al, it seems plausible that large impact events caused some H-chondrite material to be deeply buried and some material to be deposited at shallower depths. The more deeply buried material was heated the most (thus achieving higher petrologic types) and took longer to cool (thereby accounting for younger ^{40}Ar-^{39}Ar ages). The advantage of the impact scenario is that it accounts for the evidence of shock and subsequent annealing in the equilibrated OC. The old (4.50–4.56 Ga) Pb-Pb ages of the H chondrites (Trieloff et al., 2003) indicate that any postshock annealing of these rocks must have been below the closure temperature of the Pb-Pb system (~450°C).

6. CONCLUSIONS

Collisional events caused all equilibrated (petrologic type-4 to -6) OC to reach shock stages S3–S6. Those equilibrated OC that are now classified shock-stage S1 (mainly on the basis of olivine with sharp optical extinction and no planar fractures) underwent postshock annealing due to burial in proximity to rocks heated by the impact event. Those equilibrated OC that are now classified S2 (on the basis of olivine with undulose extinction but no planar fractures) were shocked to stage S3–S6, annealed to stage S1 and then shocked again to reach stage S2. It is likely that some of the equilibrated OC that are now classified shock-stage S3–S6 underwent a complicated history: they were shocked to stage S3–S6, annealed to S1, and then shocked again to S3–S6. Annealed OC buried at moderate depth were shocked again when they were excavated and launched off their parent asteroid. Some OC may have experienced multiple episodes of shock and annealing.

MIL 99301 (LL6, S1) was annealed ~4.26 Ga ago. At this late date, impacts are the only plausible heat source. Because MIL 99301 appears to have been annealed by impacts, it follows that additional type-4 to -6 S1 and S2 OC (e.g., Alta'ameem and Tuxtuac) may have been annealed by impacts. Because some type-6 S1 OC with relict shock features (i.e., Guareña, Kernouvé, Portales Valley) were annealed very early in solar-system history (4.44–4.45 Ga ago), it seems plausible that impact-induced annealing was active during the general period when most OC experienced thermal metamorphism. Collisions may thus be a major heating mechanism at least partly responsible for OC metamorphism.

Acknowledgments—I thank the curators at the Smithsonian Institution, the Institute of Meteoritics at the University of New Mexico, the Institute of Geophysics and Planetary Physics at UCLA, the Institute of Planetology at the University of Münster, The Natural History Museum (London), the University of Freiburg, the Western Australian Museum, the EUROMET working group, Open University, National Museum for the Antarctic at the University of Siena, Arizona State University, NASA Johnson Space Center, and the Antarctic Meteorite Working Group for the generous loan of numerous thin sections. I also thank J. T. Wasson for helpful comments. The manuscript benefited from helpful reviews by E. R. D. Scott, W. U. Reimold and M. Trieloff. I am grateful to associate-editor G. Herzog for his judicious handling of the manuscript. This work was supported by NASA Grant No. NAG5-4766.

Associate editor: G. Herzog

REFERENCES

Ashworth J. R. (1985) Transmission electron microscopy of L-group chondrites, 1. Natural shock effects. *Earth Planet. Sci. Lett.* **73,** 17–32.

Ashworth J. R. and Mallinson L. G. (1985) Transmission electron microscopy of L-group chondrites, 2. Experimentally annealed Kyushu. *Earth Planet. Sci. Lett.* **73,** 33–40.

Bauer J. F. (1979) Experimental shock metamorphism of mono- and polycrystalline olivine: A comparative study. *Proc. Lunar Planet. Sci. Conf.* **10,** 2573–2596.

Bennett M. E. and McSween H. Y. (1996a) Revised model calculations for the thermal histories of ordinary chondrite parent bodies. *Meteorit. Planet. Sci.* **31,** 783–792.

Bennett M. E. and McSween H. Y. (1996b) Shock features in iron-nickel metal and troilite of L-group ordinary chondrites. *Meteorit. Planet. Sci.* **31,** 255–264.

Bernatowicz T. J., Podosek F. A., Swindle T. D., and Honda M. (1988) I-Xe systematics in LL chondrites. *Geochim. Cosmochim. Acta* **52,** 1113–1121.

Binns R. A. (1970) (Mg, Fe)$_2$SiO$_4$ spinel in a meteorite. *Phys. Earth Planet. Int.* **3,** 156–160.

Binns R. A., Davis R. J., and Reed S. J. B. (1969) Ringwoodite, a natural (Mg,Fe)$_2$SiO$_4$ spinel in the Tenham meteorite. *Nature* **221,** 943–944.

Bischoff A., Rubin A. E., Keil K., and Stöffler D. (1983) Lithification of gas-rich chondrite regolith breccias by grain boundary and localized shock melting. *Earth Planet. Sci. Lett.* **66,** 1–10.

Bogard D. D., Garrison D. H., Norman M., Scott E. R. D., and Keil K. (1995) ^{39}Ar-^{40}Ar age and petrology of Chico: Large-scale impact melting on the L-chondrite parent body. *Geochim. Cosmochim. Acta* **59,** 1383–1399.

Britt D. T. and Pieters C. M. (1991) Black ordinary chondrites: An analysis of abundance and fall frequency. *Meteoritics* **26,** 279–285.

Buening D. K. and Buseck P. R. (1973) Fe-Mg lattice diffusion in olivine. *J. Geophys. Res.* **78,** 6852–6862.

Cameron A. G. W., Benz W., and Wasson J. T. (1990) Heating during asteroidal collisions (abstract). *Lunar Planet. Sci.* **21,** 155–156.

Cameron A. G. W., Benz W., and Wasson J. T. (1991) Heating during asteroidal collisions II (abstract). *Lunar Planet. Sci.* **22,** 173.

Coleman L. C. (1977) Ringwoodite and majorite in the Catherwood meteorite. *Can. Mineral.* **15,** 97–101.

Dixon E. T., Bogard D. D., and Rubin A. E. (2003) ^{39}Ar-^{40}Ar evidence for an ~4.26 Ga impact heating event on the LL parent body. *Lunar Planet. Sci.* **34,** 1108.

Dodd R. T. and Jarosewich E. (1979) Incipient melting and shock classification of L-group chondrites. *Earth Planet. Sci. Lett.* **44,** 335–340.

Ehlmann A. J., Scott E. R. D., Keil K., Mayeda T. K., Clayton R. N., Weber H. W., and Schultz L. (1988) Origin of fragmental and regolith meteorite breccias—Evidence from the Kendleton L chondrite breccia. *Proc. Lunar Planet. Sci. Conf.* **18,** 545–554.

Floran R. J., Grieve R. A. F., Phinney W. C., Warner J. L., Simonds C. H., Blanchard D. P., and Dence M. R. (1978) Manicouagan impact melt, Quebec, 1; Stratigraphy, petrology and chemistry. *J. Geophys. Res.* **83,** 2737–2759.

Fodor R. V., Keil K., and Jarosewich E. (1972) The Oro Grande, New Mexico, chondrite and its lithic inclusion. *Meteoritics* **7,** 495–507.

Fodor R. V. and Keil K. (1976) Carbonaceous and noncarbonaceous lithic fragments in the Plainview, Texas chondrite: Origin and history. *Geochim. Cosmochim. Acta* **40,** 177–189.

Fredriksson K., De Carli P., and Aaramäe A. (1963) Shock-induced veins in chondrites. *Space Res.* **3,** 974–983.

Freer R. (1981) Diffusion in silicate minerals and glasses: A data digest and guide to the literature. *Contrib. Mineral. Petrol.* **76,** 440–454.

Garrison D. H. and Bogard D. D. (2001) ^{39}Ar-^{40}Ar and space exposure ages of the unique Portales Valley H-chondrite. *Lunar Planet. Sci.* **32,** 1137.

Ghosh A. and McSween H. Y. (2000) The effect of incremental accretion on the thermal modeling of asteroid 6 Hebe (abstract). *Meteorit. Planet. Sci.* **35,** A59–A60.

Gibson R. L. (2002) Impact-induced melting of Archean granulites in the Vredefort Dome, South Africa. I: Anatexis of metapelitic granulites. *J. Metamorphic Geol.* **20,** 57–70.

Gibson R. L. and Reimold W. U. (2003) Thermal and dynamic consequences of impact—Lessons from large impact structures (abstract). In *Impact Cratering: Bridging the Gap Between Modeling and Observations*, pp. 22–23. LPI contribution 1155. Lunar and Planetary Institute.

Grady M. M. (2000) *Catalogue of Meteorites*. 5th ed. Cambridge University Press.

Grieve R. A. F., Palme H., and Plant A. G. (1980) Siderophile-rich particles in the melt rocks at the E. Clearwater Impact Structure, Quebec: Their characteristics and relationship to the impacting body. *Contrib. Mineral. Petrol.* **75,** 187–198.

Grieve R. A. F., Reny G., Gurov E. P., and Ryabenko V. A. (1987) The melt rocks of the Boltysh impact crater, Ukraine, USSR. *Contrib. Mineral. Petrol.* **96,** 56–62.

Grimm R. E. and McSween H. (1993) Heliocentric zoning of the asteroid belt by 26-Al heating. *Science* **259,** 653–655.

Haack H., Scott E. R. D., and Rasmussen K. L. (1996) Thermal and shock history of mesosiderites and their large parent asteroid. *Geochim. Cosmochim. Acta* **60,** 2609–2619.

Herbert F. (1989) Primordial electrical induction heating of asteroids. *Icarus* **78,** 402–410.

Herbert F. and Sonett C. P. (1979) Electromagnetic heating of minor planets in the early solar system. *Icarus* **40,** 484–496.

Herbert F., Sonett C. P., and Gaffey M. J. (1991) Protoplanetary thermal metamorphism: The hypothesis of electromagnetic induction in the protosolar wind. In *The Sun in Time* (eds. C. P. Sonett, M. S. Giampapa, and M. S. Matthews), pp. 710–739. University of Arizona Press.

Heymann D. and Mazor E. (1968) Noble gases in unequilibrated ordinary chondrites. *Geochim. Cosmochim. Acta* **32,** 1–19.

Housen K. R. (2003) Material motions and ejection velocities for impacts in porous targets. *Lunar Planet. Sci.* **34,** 1300.

Housen K. R. and Holsapple K. A. (1999) Impact cratering on porous low-density bodies. *Lunar Planet. Sci.* **30,** 1228.

Housen K. R. and Holsapple K. A. (2003) Impact cratering on porous asteroids. *Icarus* **163,** 102–119.

Jarosewich E. (1990) Chemical analyses of meteorites: A compilation of stony and iron meteorite analyses. *Meteoritics* **25,** 323–337.

Jurewicz A. J. G., Mittlefehldt D. W., and Jones J. H. (1995) Experimental partial melting of the St. Severin (LL) and Lost City (H) chondrites. *Geochim. Cosmochim. Acta* **59,** 391–408.

Kallemeyn G. W., Rubin A. E., Wang D., and Wasson J. T. (1989) Ordinary chondrites: Bulk compositions, classification, lithophile-element fractionations, and composition-petrographic type relationships. *Geochim. Cosmochim. Acta* **53,** 2747–2767.

Kallemeyn G. W., Rubin A. E., and Wasson J. T. (1996) The compositional classification of chondrites: VII. The R chondrite group. *Geochim. Cosmochim. Acta* **60,** 2243–2256.

Keil K. (2000) Thermal alteration of asteroids: Evidence from meteorites. *Planet. Space Sci.* **48,** 887–903.

Keil K., Stöffler D., Love S. G., and Scott E. R. D. (1997) Constraints on the role of impact heating and melting in asteroids. *Meteorit. Planet. Sci.* **32,** 349–363.

Kring D. A., Swindle T. D., Britt D. T., and Grier J. A. (1996) Cat Mountain: A meteoritic sample of an impact-melted asteroid regolith. *J. Geophys. Res.* **101,** 29353–29371.

Kring D. A., Hill D. H., Gleason J. D., Britt D. T., Consolmagno G. J., Farmer M., Wilson S., and Haag R. (1999) Portales Valley: A meteoritic sample of the brecciated and metal-veined floor of an impact crater on an H-chondrite asteroid. *Meteorit. Planet. Sci.* **34,** 663–669.

Kunz J., Falter M., and Jessberger E. K. (1997) Shocked meteorites: Argon-40-argon-39 evidence for multiple impacts. *Meteorit. Planet. Sci.* **32,** 647–670.

Lambert P., Lewis C., and Moore C. B. (1984) Repeated shock and thermal metamorphism of the Abernathy meteorite. *Meteoritics* **19,** 29–48.

Leroux H., Doukhan J.-C., and Guyot F. (1996) An analytical electronmicroscopy (AEM) investigation of opaque inclusions in some type-6 ordinary chondrites. *Meteorit. Planet. Sci.* **31,** 767–776.

Liu L.-G. (1978) High-pressure phase transformations of albite, jadeite and nepheline. *Earth Planet. Sci. Lett.* **37,** 438–444.

Marti K. (1967) trapped xenon and the classification of chondrites. *Earth Planet. Sci. Lett.* **2,** 193–196.

Mason B. and Wiik H. B. (1962) The Renazzo meteorite. *Am. Mus. Novitates* **2106,** 1–11.

McSween H. Y. (1977) Carbonaceous chondrites of the Ornans type: A metamorphic sequence. *Geochim. Cosmochim. Acta* **41,** 477–491.

McSween H. Y. (1999) *Meteorites and Their Parent Planets* 2nd ed. Cambridge University Press.

McSween H. Y., Taylor L. A., and Lipschutz M. E. (1978) Metamorphic effects in experimentally heated Krymka (L3) chondrite. *Proc. Lunar Planet. Sci. Conf.* **9,** 1437–1447.

McSween H. Y., Ghosh A., Grimm R. E., Wilson L., and Young E. D. (2002) Thermal evolution models of asteroids. In *Asteroids III* (eds. W. F. Bottke, A. Cellino, P. Paolicchi, and R. P. Binzel), pp. 559–571. University of Arizona Press.

Melosh H. J. (1989) *Impact Cratering: A Geologic Process*. Oxford University Press.

Mittlefehldt D. W. and Lindstrom M. M. (2001) Petrology and geochemistry of Patuxent Range 91501, a clast-poor impact melt from the L-chondrite parent body and Lewis Cliff 88663, an L7 chondrite. *Meteorit. Planet. Sci.* **36,** 439–457.

Mostefaoui S., Lugmair G. W., Hoppe P., and El Goresy A. (2003) Evidence for live iron-60 in Semarkona and Chervony Kut: A nanoSIMS study. *Lunar Planet. Sci.* **34,** 1585.

Pellas P. and Storzer D. (1981) ^{244}Pu fission track thermometry and its application to stony meteorites. *Proc. R. Soc. Lond.* **374,** 253–270.

Pellas P. and Fiéni C. (1988) Thermal histories of ordinary chondrite parent asteroids (abstract). *Lunar Planet. Sci.* **19,** 915–916.

Pellas P., Fiéni C., Trieloff M., and Jessberger E. K. (1990) Metamorphism intervals of equilibrated H and LL chondrites as defined by ^{244}Pu chronometry and Ar-Ar ages (abstract). *Meteoritics* **25,** 397.

Reeves H. and Audouze J. (1968) Early heat generation in meteorites. *Earth Planet. Sci. Lett.* **4,** 135–141.

Reimold W. U., Barr J. M., Grieve R. A. F., and Durrheim R. J. (1990) Geochemistry of the melt and country rocks of the Lake St. Martin impact structure, Manitoba, Canada. *Geochim. Cosmochim. Acta* **54,** 2093–2111.

Reimold W. U. and Colliston W. P. (1994) Pseudotachylites of the Vredefort Dome and the surrounding Witwatersrand Basin, South Africa. Special Paper 293, pp. 177–196. Geological Society of America.

Reisener R. J. and Goldstein J. I. (in press) The formation of zoned and unzoned metal particles in low-shock types 4–6 ordinary chondrites. *Meteorit. Planet. Sci.* **38,** in press.

Rubin A. E. (1985) Impact melt products of chondritic material. *Rev. Geophys.* **23,** 277–300.

Rubin A. E. (1990) Kamacite and olivine in ordinary chondrites: Intergroup and intragroup relationships. *Geochim. Cosmochim. Acta* **54,** 1217–1232.

Rubin A. E. (1992) A shock-metamorphic model for silicate darkening and compositionally variable plagioclase in CK and ordinary chondrites. *Geochim. Cosmochim. Acta* **56,** 1705–1714.
Rubin A. E. (1994) Metallic copper in ordinary chondrites. *Meteoritics* **29,** 93–98.
Rubin A. E. (1995a) Fractionation of refractory siderophile elements in metal from the Rose City meteorite. *Meteoritics* **30,** 412–417.
Rubin A. E. (1995b) Petrologic evidence for collisional heating of chondritic asteroids. *Icarus* **113,** 156–167.
Rubin A. E. (1999) Formation of large metal nodules in ordinary chondrites. *J. Geophys. Res.* **104,** 30799–30804.
Rubin A. E. (2002) Post-shock annealing of MIL99301 (LL6): Implications for impact heating of ordinary chondrites. *Geochim. Cosmochim. Acta* **66,** 3327–3337.
Rubin A. E. (2003) Chromite-plagioclase assemblages as a new shock indicator; Implications for the shock and thermal histories of ordinary chondrites. *Geochim. Cosmochim. Acta* **67**, in press.
Rubin A. E. and Jones R. H. (2003) Spade: An H chondrite impact-melt breccia that experienced post-shock annealing. *Met. Planet. Sci.* **38,** 2695–2709.
Rubin A. E., Rehfeldt A., Peterson E., Keil K., and Jarosewich E. (1983) Fragmental breccias and the collisional evolution of ordinary chondrite parent bodies. *Meteoritics* **18,** 179–196.
Rubin A. E. and Read W. F. (1984) The Brownell and Ness County (1894) L6 chondrites: Further sorting out of Ness County meteorites. *Meteoritics* **19,** 153–160.
Rubin A. E., Ulff-Møller F., Wasson J. T., and Carlson W. D. (2001) The Portales. Valley meteorite breccia: Evidence for impact-induced melting and metamorphism of an ordinary chondrite. *Geochim. Cosmochim. Acta* **65,** 323–342.
Rubin A. E., Zolensky M. E., and Bodnar R. J. (2002) The halite-bearing Zag and Monahans. (1998) meteorite breccias: Shock metamorphism, thermal metamorphism, and aqueous alteration on the H-chondrite parent body. *Meteorit. Planet. Sci.* **37,** 125–141.
Schmitt R. T., Deutsch A., and Stöffler D. (1993) Shock effects in experimentally shocked samples of the H6 chondrite Kernouvé (abstract). *Meteoritics* **28,** 431–432.
Schmitt R. T., Deutsch A., and Stöffler D. (1994) Shock recovery experiments with the H6 chondrite Kernouvé at preshock temperatures of 293 and 920 K (abstract). *Meteoritics* **29,** 529–530.
Schmitt R. T. and Stöffler D. (1995) Classification of chondrites (abstract). *Meteoritics* **30,** 574–575.
Schuraytz B. C., Sharpton V. L., and Marín L. E. (1994) Petrology of impact-melt rocks at the Chicxulub multiring basin, Yucatán, Mexico. *Geology* **22,** 868–872.
Scott E. R. D. (1982) Origin of rapidly solidified metal-troilite grains in chondrites and iron meteorites. *Geochim. Cosmochim. Acta* **46,** 813–823.
Scott E. R. D., Lusby D., and Keil K. (1985) Ubiquitous brecciation after metamorphism in equilibrated ordinary chondrites. *Proc. Lunar Planet. Sci. Conf.* **16,** D137–D148.
Scott E. R. D., Keil K., and Stöffler D. (1992) Shock metamorphism of carbonaceous chondrites. *Geochim. Cosmochim. Acta* **56,** 4281–4293.
Sears D. W. and Axon H. J. (1975) The metal content of common chondrites (abstract). *Meteoritics* **10,** 486–487.
Shimazu H. and Terasawa T. (1995) Electromagnetic induction heating of meteorite parent bodies by the primordial solar wind. *J. Geophys. Res.* **100,** 16923–16930.
Shukolyukov A. and Lugmair G. W. (1993) ^{60}Fe in eucrites. *Earth Planet. Sci. Lett.* **119,** 159–166.
Smith J. V. and Mason B. (1970) Pyroxene-garnet transformation in Coorara meteorite. *Science* **168,** 832–833.
Smith B. A. and Goldstein J. I. (1977) The metallic microstructures and thermal histories of severely reheated chondrites. *Geochim. Cosmochim. Acta* **41,** 1061–1072.
Sonett C. P., Colburn D. S., Schwartz K., and Keil K. (1970) The melting of asteroidal-sized bodies by unipolar dynamo induction from a primordial T Tauri sun. *Astrophys. Space Phys.* **7,** 446–488.
Stewart S. T. and Ahrens T. J. (1999) Porosity effects on impact processes in solar system materials. *Lunar Planet. Sci.* **30,** 2020.
Stöffler D., Keil K., and Scott E. R. D. (1991) Shock metamorphism of ordinary chondrites. *Geochim. Cosmochim. Acta* **55,** 3845–3867.
Takeda H., Huston T. J., and Lipschutz M. E. (1984) On the chondrite–achondrite transition: Mineralogy and chemistry of Yamato 74160 (LL7). *Earth Planet. Sci. Lett.* **71,** 329–339.
Tandon S. N. and Wasson J. T. (1968) Gallium, germanium, indium and iridium variations in a suite of L-group chondrites. *Geochim. Cosmochim. Acta* **32,** 1087–1109.
Taylor G. J. and Heymann D. (1970) Electron microprobe study of metal particles in the Kingfisher meteorite. *Geochim. Cosmochim. Acta* **34,** 677–687.
Taylor G. J., Keil K., Berkley J. L., and Lange D. E. (1979) The Shaw meteorite: History of a chondrite consisting of impact-melted and metamorphic lithologies. *Geochim. Cosmochim. Acta* **43,** 323–337.
Taylor G. J., Maggiore P., Scott E. R. D., Rubin A. E., and Keil K. (1987) Original structures, and fragmentation and reassembly histories of asteroids: Evidence from meteorites. *Icarus* **69,** 1–13.
Trieloff M., Jessberger E. K., and Oehm J. (1989) Ar-Ar ages of LL chondrites (abstract). *Meteoritics* **24,** 332.
Trieloff M., Kunz J., and Jessberger E. K. (1994) High-resolution ^{40}Ar-^{39}Ar dating of K-rich chondritic inclusions (abstract). *Meteoritics* **29,** 541–542.
Trieloff M., Jessberger E. K., Herrwerth I., Hopp J., Fiéni C., Ghélls M., Bourot-Denise M., and Pellas P. (2003) Structure and thermal history of the H-chondrite parent asteroid revealed by thermochronometry. *Nature* **422,** 502–506.
Turner G., Enright M. C., and Cadogan P. H. (1978) The early history of chondrite parent bodies inferred from ^{40}Ar-^{39}Ar ages. *Proc. Lunar Planet. Sci. Conf.* **9,** 989–1025.
Wasson J. T., Benz W., and Rubin A. E. (1987) Heating of primitive, asteroid-size bodies by large impacts. *Meteoritics* **22,** 525–526.
Widom E., Rubin A. E., and Wasson J. T. (1986) Composition and formation of metal nodules and veins in ordinary chondrites. *Geochim. Cosmochim. Acta* **50,** 1989–1995.
Wilkening L. L. (1978) Tysnes Island: An unusual clast composed of solidified, immiscible, Fe-FeS and silicate melt. *Meteoritics* **13,** 1–9.
Wlotzka F. (1993) A weathering scale for the ordinary chondrites (abstract). *Meteoritics* **28,** 460.
Wood J. A. and Pellas P. (1991) What heated the parent meteorite planets?. In *The Sun in Time* (eds. C. P. Sonett, M. S. Giampapa, and M. S. Matthews), pp. 740–760. Univeristy of Arizona Press.
Xie X., Minitti M. E., Chen M., Mao H.-K., Wang D., Shu J., and Fei Y. (2002) Natural high-pressure polymorph of merrillite in the shock veins of the Suizhou meteorite. *Geochim. Cosmochim. Acta* **66,** 2439–2444.
Yamaguchi A., Scott E. R. D., and Keil K. (1998) Origin of unusual impact melt rocks, Yamato-790964 and -790143 (LL-chondrites). *Ant. Met. Res.* **11,** 18–31.
Zähringer J. (1966) Primordial argon and the metamorphism of chondrites. *Earth Planet. Sci. Lett.* **1,** 379–382.